

# JGR Atmospheres

## RESEARCH ARTICLE

10.1029/2021JD035988

### Key Points:

- The wintertime CUHII in Beijing is sensitive to Synoptic Weather Patterns (SWPs) at diurnal and interannual scale
- Temporal variation in the strength of CUHII is closely linked with SWPs, while spatial pattern of CUHII is mainly shaped by LCZs
- Daily amplitudes and peaks of CUHII vary under different SWPs

### Correspondence to:

G. Ren,  
guoyoo@cma.gov.cn

### Citation:

Yang, Y., Guo, M., Ren, G., Liu, S., Zong, L., Zhang, Y., et al. (2022). Modulation of wintertime canopy urban heat island (CUHI) intensity in Beijing by synoptic weather pattern in planetary boundary layer. *Journal of Geophysical Research: Atmospheres*, 127, e2021JD035988. <https://doi.org/10.1029/2021JD035988>

Received 10 OCT 2021

Accepted 4 APR 2022

### Author Contributions:

**Conceptualization:** Yuanjian Yang,

Guoyu Ren

**Data curation:** Min Guo, Shuhong Liu, Lian Zong, Yanhao Zhang

**Formal analysis:** Yuanjian Yang, Min Guo, Guoyu Ren, Shuhong Liu, Lian Zong, Ying Zhang

**Funding acquisition:** Yuanjian Yang

**Methodology:** Yuanjian Yang, Shuhong Liu, Lian Zong, Yucong Miao, Ying Zhang

**Project Administration:** Guoyu Ren

**Resources:** Zuofang Zheng

**Software:** Yuanjian Yang, Min Guo, Shuhong Liu, Lian Zong, Zuofang Zheng, Yucong Miao, Ying Zhang

**Supervision:** Guoyu Ren


**Validation:** Yuanjian Yang, Min Guo, Shuhong Liu, Lian Zong, Zuofang Zheng, Yucong Miao, Ying Zhang

**Visualization:** Yuanjian Yang, Min Guo, Shuhong Liu, Yanhao Zhang

**Writing – original draft:** Yuanjian Yang, Zuofang Zheng

**Writing – review & editing:** Yuanjian Yang, Min Guo, Guoyu Ren, Lian Zong

## Modulation of Wintertime Canopy Urban Heat Island (CUHI) Intensity in Beijing by Synoptic Weather Pattern in Planetary Boundary Layer

Yuanjian Yang<sup>1</sup> , Min Guo<sup>1</sup>, Guoyu Ren<sup>2,3</sup> , Shuhong Liu<sup>1,4</sup>, Lian Zong<sup>1</sup>, Yanhao Zhang<sup>1</sup>, Zuofang Zheng<sup>5</sup>, Yucong Miao<sup>6</sup>, and Ying Zhang<sup>7</sup>

<sup>1</sup>Collaborative Innovation Centre on Forecast and Evaluation of Meteorological Disasters | Key Laboratory for Aerosol-Cloud-Precipitation of China Meteorological Administration | School of Atmospheric Physics, Nanjing University of Information Science & Technology, Nanjing, China, <sup>2</sup>Department of Atmospheric Science, School of Environmental Studies, China University of Geosciences, Wuhan, China, <sup>3</sup>Laboratory for Climate Studies, National Climate Center, China Meteorological Administration, Beijing, China, <sup>4</sup>Linyi Meteorological Observatory, Linyi Meteorological Bureau, Linyi, China, <sup>5</sup>Institute of Urban Meteorology, China Meteorological Administration, Beijing, China, <sup>6</sup>Chinese Academy of Meteorological Sciences, Beijing, China, <sup>7</sup>State Key Laboratory of Atmospheric Boundary Layer Physics and Atmospheric Chemistry (LAPC), Institute of Atmospheric Physics, Chinese Academy of Sciences, Beijing, China

**Abstract** Studying the spatiotemporal variations of the urban heat island (UHI) effect and its cause is important towards understanding urban climate change, planning and green development, and disaster mitigation. In this paper, by using surface observations and reanalysis data with objective classification of synoptic weather patterns (SWPs), we analyze the associations between canopy UHI intensity (CUHI) and SWPs in the planetary boundary layer (PBL) and their potential drivers during wintertime of the period 2012–2017. Six dominant types of SWP are identified as follows: In the case of Types 3, 4, and 6, weak high-pressure systems exist to the south of Beijing, resulting in weak southerly winds with low PBL height, large cloud coverage and high relative humidity (RH). These conditions are generally conducive to a strengthening of the CUHII. In contrast, under Types 1, 2, and 5, high-pressure systems are located to the northwest of Beijing, and the associated strong northwesterly flows of dry and cold air strengthen the boundary layer mixing process, resulting in large wind speed and low RH. This is conducive to a weakening of the CUHII. In general, our work reveals the impacts of SWPs on the strength of CUHII mainly via the modulation of local weather conditions at diurnal and interannual scales, while spatial pattern of CUHII is largely dominated by local climate zones. Our findings have implications for CUHII forecasts, as well as impact assessments and policymaking in the context of UHI-related energy conservation in winter over high-density urban areas on the synoptic scale.

## 1. Introduction

The urban heat island (UHI) phenomenon refers to enhanced air/surface temperatures in urban areas with respect to their surrounding rural areas (Oke et al., 2017; Oke & Maxwell, 1975; Rizwan et al., 2008; Roth, 2007), which is the most obvious characteristic of the urban thermal environment. The UHI effect has become one of the dominant factors affecting the urban climate and ecological environment (Crutzen, 2004; Oke et al., 2017; Ren, 2015). In particular, the impacts that UHIs have on heat waves and extreme climate events (Li & Bouzeid, 2013; Luo & Lau, 2017; X. C. Yang et al., 2017), air quality (L. Chen et al., 2018; Velasco & Roth, 2012; Zheng et al., 2018), energy consumption (Kolokotroni et al., 2012; Sun & Augenbroe, 2014), and human health threats (Hu et al., 2019; Luo & Lau, 2018; Yang, Gao, et al., 2019) cannot be ignored. Therefore, studying the temporal and spatial evolution of UHI intensity and its formation mechanism is of great significance for understanding the characteristics of urban climate change, urban planning and green development, and disaster prevention and mitigation (Max et al., 2020; Oke et al., 2017; Roth, 2007; Yang, Zhang, et al., 2020; Zhao et al., 2014).

Beijing, the capital of China, is an inland city with a high population density located in the typical north-temperate, semi-humid and continental monsoon climate zone. Rapid urbanization has induced a significant canopy UHI (CUHI) effect in Beijing in recent years (W. Liu et al., 2007; Ren et al., 2007; Yan et al., 2010; Yang, Ren & Liu, 2013; Yang, Zheng, et al., 2020). Understanding the CUHI effect in Beijing is important to regional climate and environmental issues owing to the strong canopy UHI intensity (CUHII) caused by the large population density and its associated high energy consumption. Until now, studies on the CUHI in Beijing have mainly

concentrated on its periodic variation, spatial distribution, vertical structure with local circulation, and formation reasons (S. H. Liu et al., 2009; Wang et al., 2017; Yang, Ren, & Hou, 2019), as well as its impacts on climatic-environment and health (L. Chen et al., 2018; Yang, Zheng, et al., 2020; L. Zhang et al., 2011; Zheng et al., 2020). The diurnal variation of the CUHI in Beijing is characterized by strong CUHI at night and early morning, and weak CUHI during daytime showing a V-shaped fluctuation (W. Liu et al., 2007; Xie et al., 2006; Yang, Ren, & Liu, 2013). At the seasonal scale, the variations of seasonal-mean CUHIs mainly follow the pattern of summer < spring < autumn < winter (W. Liu et al., 2007; Xie et al., 2006; Yang, Ren, & Liu, 2013). This is partially because there is more anthropogenic heat released in winter than in summer, and the anthropogenic heat release in urban areas suppress the development of the boundary layer, which is more helpful to enhance CUHI (Jauregui et al., 1992; Oke et al., 1991; K. Wang et al., 2017). On the multi-decadal scale, the CUHI has increased significantly in the past decades, and its contribution to the warming of the average and minimum temperatures around the observational stations of Beijing urban areas cannot be ignored (Ren et al., 2007). The factors driving the CUHI changes in Beijing urban areas are complex and diverse, but can broadly be categorized into natural-type factors (local meteorological factors such as the winds, cloud cover, rainfall, relative humidity [RH], etc.) and anthropogenic-type factors (i.e., anthropogenic activities such as emissions of anthropogenic heat and aerosols, as well as land use/land cover changes related to rapid urbanization, etc.) (Ren et al., 2007; Yang, Ren & Hou, 2019; Yang, Zheng, et al., 2020; Zheng et al., 2018).

As another important driver, certain synoptic weather patterns (SWPs) can cause noticeable changes in CUHI via their modulation of local meteorological factors. For instance, high-pressure systems in summer can suppress the development of the planetary boundary layer (PBL) and induce calm and cloudless conditions that are conducive to CUHI intensification (Craig & Bornstein, 2002; Stewart & Oke, 2012). Until now, however, most previous studies on the CUHI changes in Beijing have mainly focused on the multi-decadal, interannual, seasonal or diurnal scales (Ren et al., 2007; K. Wang et al., 2017; Xie et al., 2006; Yang, Ren, & Hou, 2019), leaving a gap in knowledge with respect to the variations at the synoptic scale and their potential driving forces. Particularly, the PBL height in winter is the lowest among four seasons (Miao et al., 2015), which are conducive to CUHI intensification. In general, there are still three issues with respect to the wintertime CUHI in Beijing that have yet to be fully understood: (a) what are the characteristics of the CUHI under different SWPs in the PBL? (b) on the synoptic scale, how important are the potential factors of influence in shaping the spatial and temporal distribution of the CUHI in Beijing? (c) are there any associations between the diurnal/interannual variations of the CUHI and those of the SWPs in the PBL?

In the present study, to address these three issues, we systematically analyze the associations between the wintertime CUHI and SWP in the PBL in Beijing by using multi-source meteorological and environmental data together objective classification of the SWPs. Following this introduction, Section 2 describes the various observational data and methods used in the study. Section 3 examines interannual and diurnal variations of the CUHI and their associations with different SWPs. The possible drivers are then discussed in Section 4, followed by concluding remarks in Section 5.

## 2. Data and Methods

Surface air temperature (SAT), daily maximum surface air temperature ( $T_{\max}$ ), minimum surface air temperature ( $T_{\min}$ ), RH, and surface wind speed (SWS) data recorded at 295 automatic weather stations in Beijing (see Figure 1a) (122 stations are within the Sixth Ring Road) during 2012–2017 were collected from the China Meteorological Data Service Center, China meteorological Administration (CMA), which are available at <http://data.cma.cn/en>. The diurnal temperature range (DTR) describes the difference between  $T_{\max}$  and  $T_{\min}$ . Daily meteorological data have been quality controlled and homogenized using the method described by Xu et al. (2013). The PM<sub>2.5</sub> data are from the national 24-hr continuous air quality observation published by the China Environmental Monitoring Station (<http://www.cnemc.cn/>).

The radiation data used in this study are from the Beijing 325-m meteorological tower, which is located at an urban site at the Institute of Atmospheric Physics (IAP), Chinese Academy of Sciences (CAS) (39.97°N, 116.37°E). The downward shortwave radiation (DSR), and downward longwave radiation (DLR) are collected using the downward-pointing pyranometers at a height of 47-m to measure the component radiation.

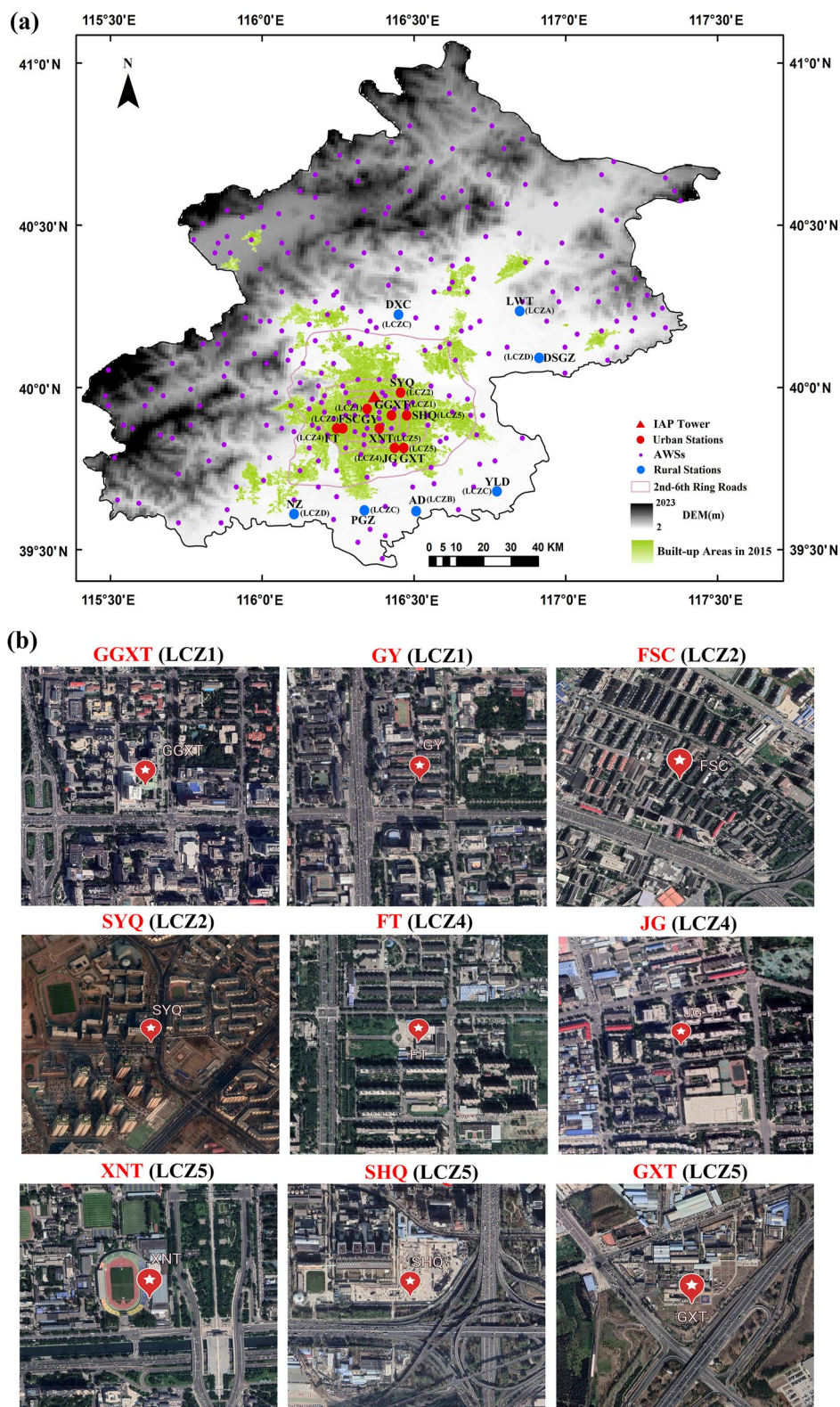


**Figure 1.** (a) The spatial distribution of meteorological stations and urban stations as outlined by the 5th Ring Road (purple solid circles; from the inner to outer lines are from the 2nd to 6th Ring Road) and the 7 rural stations outside of the 6th Ring Road (abbreviations for the station names are: YLD, Yong Le Dian; PGZ, Pang Ge Zhuang; AD, An Ding; NZ, Nan Zhao; DSGZ, Da Sun Ge Zhuang; LWT, Long Wan Tun; DXC, Dong Xin Cheng). (b) The specific urban canopy structure of the 9 city stations.



**Table 1**  
*Geographical Locations of the Urban and Reference (Rural) Stations*

Station	Lon (°E)	Lat (°N)	Altitude (m)	Station types	Local climate zone
GGXT	116.43	39.91	48	Urban	LCZ1
GY	116.35	39.93	55	Urban	LCZ1
FSC	116.27	39.87	54	Urban	LCZ2
SYQ	116.46	39.98	40	Urban	LCZ2
FT	116.25	39.87	57	Urban	LCZ4
JG	116.44	39.81	36	Urban	LCZ4
GXT	116.47	39.80	32.5	Urban	LCZ5
SHQ	116.48	39.91	40	Urban	LCZ5
XNT	116.39	39.87	49	Urban	LCZ5
LWT	116.85	40.23	52	Rural	LCZA
AD	116.51	39.61	24	Rural	LCZB
DXC	116.45	40.22	49	Rural	LCZC
PGZ	116.34	39.61	34	Rural	LCZC
YLD	116.78	39.67	17	Rural	LCZC
DSGZ	116.92	40.08	35	Rural	LCZD
NZ	116.11	39.60	34	Rural	LCZD

The Local Climate Zone (LCZ) framework is one of the most important climate classifications used in UHI studies (Max et al., 2020; Stewart & Oke, 2012). To investigate the influences of standard and subclasses of LCZ on the spatial distribution of the UHI Beijing city, nine stations located inside Beijing's 5th Ring Road over a diversity of urban landscapes with different LCZs, and seven rural stations located in the suburban areas, were selected as urban stations and reference stations, respectively, based on the previous studies (Yang, Ren, & Liu, 2013; Zong, Liu, et al., 2021) (Figure 1a and Table 1). The urban canopy structures around the nine urban stations are shown in Figure 1b (the image is from Google Earth). As for reference rural stations, they are mainly located over short grass, scrubland or cropland (Figure 2). The CUHII is defined as the difference between the SAT at each urban station and the average SAT of the eight rural stations. Note that the altitude differences between the urban and rural stations are marginal (Figure 2), which have little influence on the CUHII calculations. In this study, Anthropogenic Heat Flux (AHF) in Beijing was estimated with satellite data using the RAHF (Refined Anthropogenic Heat Flux) model, which can clearly demonstrate the spatial distribution of AHF at a 1-km resolution based on multisource remote sensing data and energy consumption statistics, including anthropogenic heat sources of industrial activities, heating and cooling of buildings, human metabolism, and vehicle exhaust (S. S. Chen et al., 2019; L. Wang et al., 2020). Mean AHF in a buffer area with a 5-km radius around each station was calculated, according to our previous study (Yang, Zheng, et al., 2020).

For synoptic analysis of the CUHII in winter, we used the geopotential height field and wind field data at 925 hPa from the National Centers for Environmental Prediction (NCEP) global Final (FNL) reanalysis data set on a  $1^\circ \times 1^\circ$  latitude/longitude grid during the study period, which are available at <http://rda.ucar.edu/datasets/ds083.2/> (National Centers, 2000; Smith et al., 2014). The T-mode principal component analysis (T-PCA) method, as an objective mathematical computer-based method, was employed to classify the SWPs in the PBL of winter. The T-PCA analysis module of the COST733 software (<http://cost733.met.no/>) developed by the European Scientific and Technical Research Cooperation was used to classify the daily synoptic circulation patterns based on the 925 hPa geopotential height field. The cost733class program is a FORTRAN software package consisting of several modules for classification, evaluation and comparison of weather and circulation patterns (Ning et al., 2018, 2019; Zong, Yang, et al., 2021). T-PCA would standardize the weather data spatially and split them into 10 subsets at first. Then, the principal components (PCs) of weather information are estimated by applying singular value decomposition, and the PC score for each subset can be calculated after oblique rotation. Finally, the resultant subset with the highest sum will be selected by comparing 10 subsets according to contingency tables, and its types can be output as well (Miao et al., 2017; Philipp et al., 2014). The explained cluster variance (ECV) was selected to assess the performance of synoptic classification and determine the number of classes in this study (Hoffmann & SchlöNzen, 2013; Ning et al., 2019; Philipp et al., 2014). In addition, to discuss the influence of total cloud cover (TCC), PBLH, wind at 925-hPa level, and precipitation on the CUHII, we also used high-resolution ( $0.25^\circ \times 0.25^\circ$  latitude/longitude grid) hourly ERA5 reanalysis data of these variables (<https://cds.climate.copernicus.eu/cdsapp#!/dataset/reanalysis-era5-single-levels?tab=form>) (Muñoz-Sabater et al., 2021). The frequency for each SWP type in every month is defined as the days of occurrences divided by total days.

### 3. Results

#### 3.1. Synoptic Classification and Corresponding CUHII Distribution

Based on the T-PCA results, six dominant types of SWP during wintertime of the period 2012–2017 can be identified as follows:

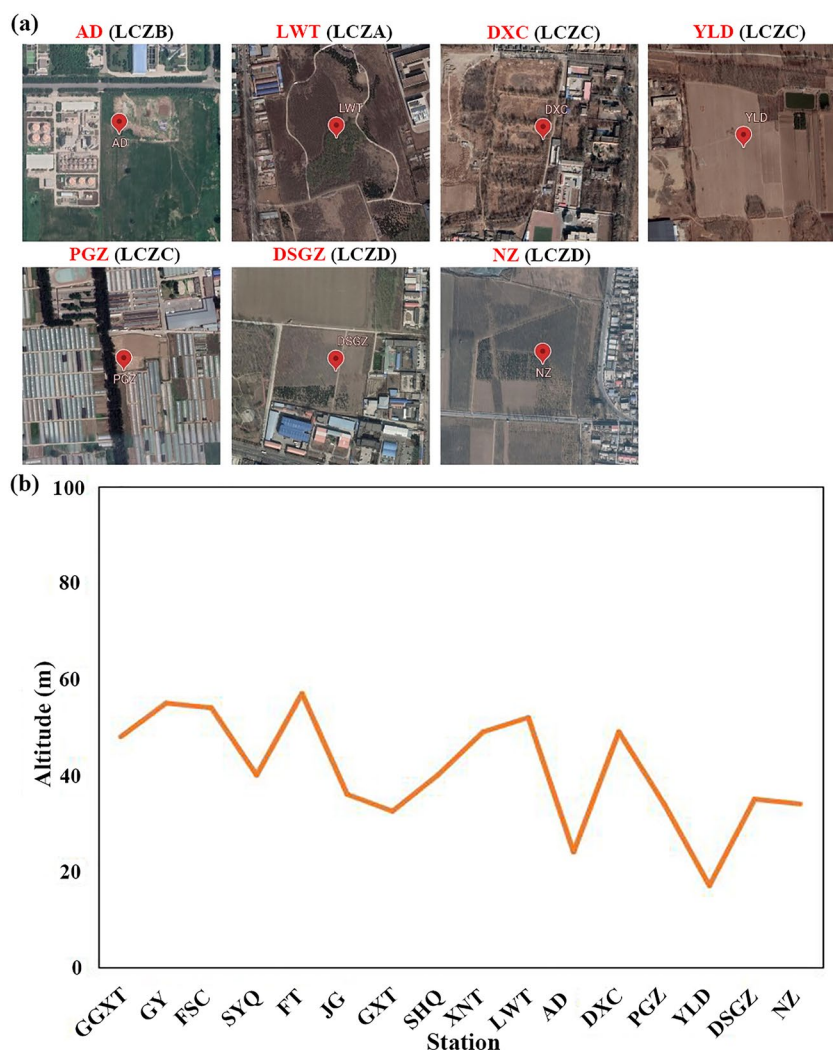


**Figure 2.** The specific land use/land cover of the seven rural stations and (b) altitude at urban and rural stations in Beijing.

1. Type 1. Beijing is located at the front of the Mongolian high pressure at 925 hPa, and its eastern part is controlled by the northeast low pressure. Under the confluence of the high- and low-pressure system, there is a northwest jet in the PBL over Beijing (Figure 3a).
2. Type 2. Beijing is located at the bottom of the high-pressure center, with prevailing north-northwest airflow in the PBL (Figure 3b).
3. Type 3. There low pressure to the northeast of Beijing and weak high pressure to the southeast, together with weak westerly winds over Beijing (Figure 3c).
4. Type 4. There is a weak high-pressure system to the southeast of Beijing, resulting in prevailing southwesterly winds over Beijing (Figure 3d).
5. Type 5. High pressure is located to the northwest of Beijing, and northwesterly winds prevail over the city (Figure 3e).
6. Type 6. There is weak high pressure to the southwest of Beijing, with prevailing southwesterly winds (Figure 3f).

The occurrence frequency and average CUHI of each SWP in Beijing are also given in Figure 3 and Table 2, indicating that Type 1 has the highest occurrence frequency (47.6%), while its CUHII is about 1.88°C. Stronger mean UHI intensities of 2.07°C, 2.03°C, and 1.98°C appear mainly in Types 3, 4, and 6, respectively, while lower ones are associated with Type 2 (1.58°C) and Type 5 (1.76°C), as shown in Table 2.

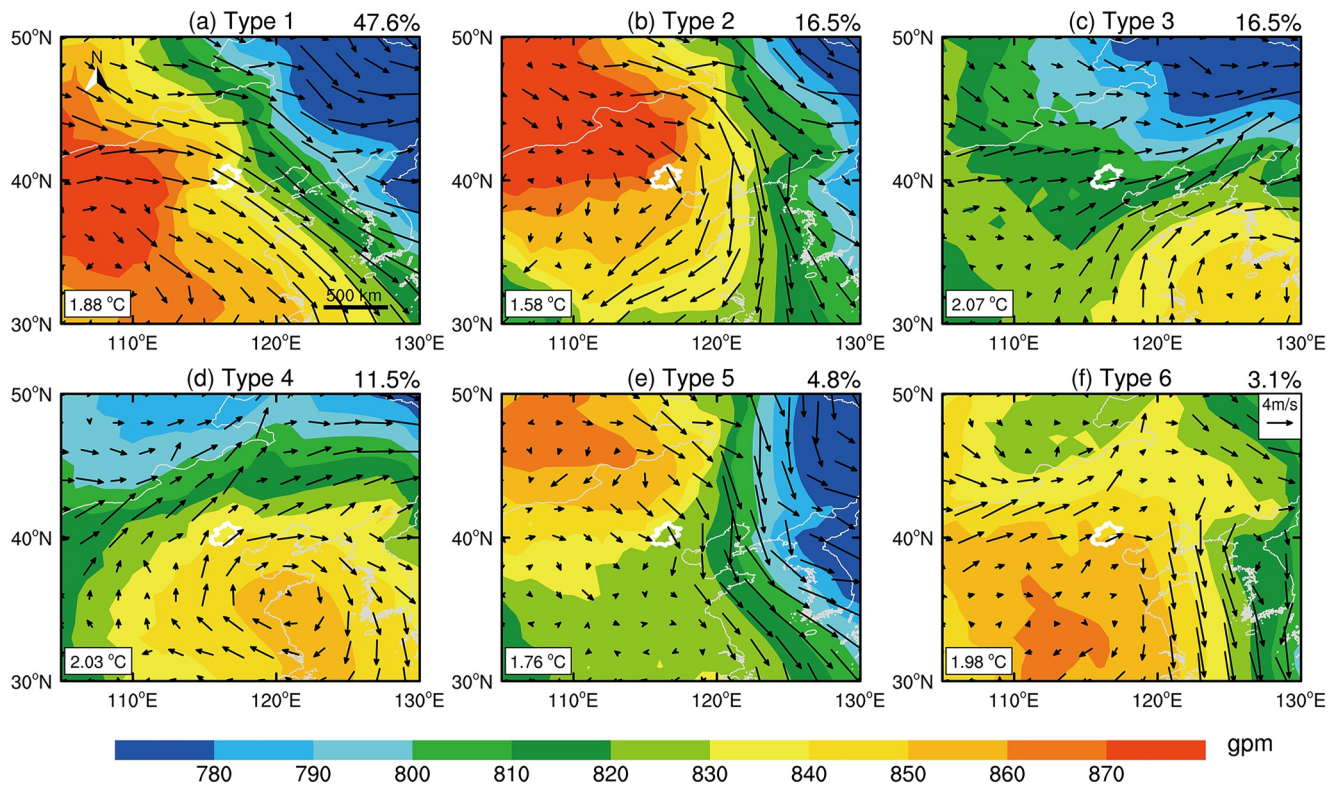


**Figure 3.** The 925-hPa wind (vectors) and geopotential height (shading) patterns based on objective classification (see text for details) in six weather types [(a–f), respectively]. The small white contour is the area of Beijing; the numbers in the bottom-left/top-right corner of each panel indicate the mean CUHI (urban heat island) intensity/frequency of occurrence in each synoptic weather pattern (SWP).

To further analyze the spatial distribution characteristics of the CUHI, Figure 4 shows the average distribution of the CUHI, surface wind vector and RH in winter under each SWP. In general, all warm CUHI centers are well matched in economically developed and densely populated urban areas in all types, while there are obvious differences in the range and intensity of the CUHI between these six types with different surface RHs and wind vectors (Figure 4). In Types 3, 4, and 6, relative to the other three types, there are larger areas of CUHI > 0°C, and the CUHI effects are more obvious, with larger areas showing strong CUHI in the center area exceeding 2.5°C (Figures 4c, 4d and 4f). The wind speeds are lower, with average values < 0.9 m/s, while the RH is higher than 50% over most areas (Figures 4c, 4d and 4f, and Table 2). On the contrary, In Types 1, 2, and 5, the CUHIs are weaker in strength and the areas of CUHI > 0°C are smaller, accompanied by stronger northerly winds with average wind speeds > 1.1 m/s, and the RH near the urban center is maintained below 40% (Figures 4a, 4b and 4e, and Table 2).

**Table 2**

*CUHI<sub>Tave</sub>, Relative Humidity (RH), Surface Wind Speed (SWS) and Planetary Boundary Layer (PBLH) Under Six Weather Types in Beijing*

Type	Total days	CUHI <sub>Tave</sub> (°C)	RH (%)	SWS (m/s)	PBLH <sub>mean</sub> (m)
1	258	1.88	33.4	1.7	587.9
2	89	1.58	38.3	1.7	490.3
3	89	2.07	58.1	0.9	347.3
4	62	2.03	49.8	1.1	264.0
5	26	1.76	36.5	1.5	461.5
6	17	1.98	53.0	1.2	288.5

### 3.2. Diurnal Variations in CUHI Under Different SWPs

To explore the modulation of the diurnal variation of the CUHI by different SWPs, we examine the diurnal variation characteristics of the CUHI under the aforementioned six different types (Figure 5a). The patterns of diurnal variation under the six weather types are basically similar, with their peaks mainly in the early morning [0400–0800 Beijing time (BJT)]. The diurnal variation of CUHI can be divided into four stages as follows: (a) stably high CUHI (>2.5°C) from early evening to early morning (2000–0800 BJT); (b) sharp drop (~3°C) in the morning (0900–1100 BJT); (c) stably lower CUHI (<1°C) in the afternoon (1200–1700 BJT); and (d) rapid increase (~2°C) in the early evening (1800–1900 BJT). This diurnal



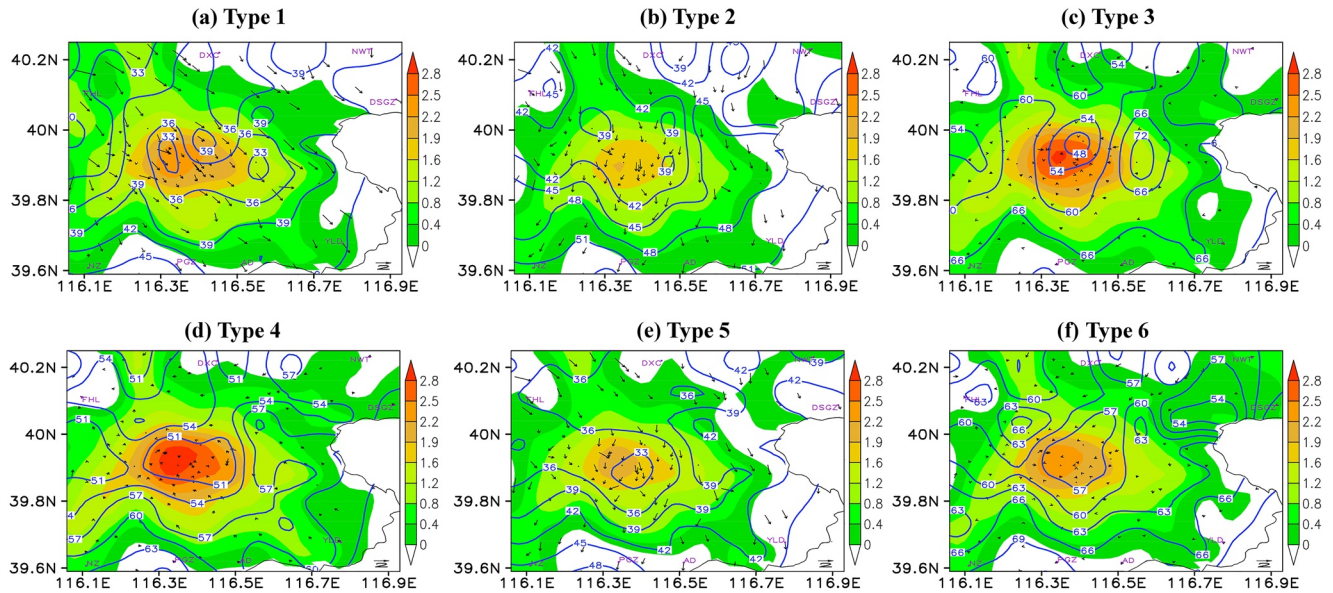


**Figure 4.** Average distribution of the CUHII (CUHII intensity, shading), 10-m-height wind vector (arrows) and RH (relative humidity, contours) in winter under the six SWPs in Beijing.

variation pattern is highly consistent with the mean pattern reported in previous studies (Cui et al., 2017; Yang, Ren, & Liu, 2013).

This diurnal pattern is caused by differences in PBLH with weather stability between daytime and nighttime, and the differences of heat stored capacity between urban and rural buildings during daytime and nighttime. At night, more stable weather conditions with a low PBLH (Figure 5b), in combination with the aerosol–cloud interactions will weaken the heat exchange and strengthen the accumulation of heat in urban areas (Yang, Zheng, et al., 2020), while the openness of rural areas will promote radiation cooling, resulting in a larger CUHII (Table 3 and Figure 4). During daytime, owing to the higher PBL (Figure 5b) and aerosol cooling effects in urban areas, the CUHII becomes smaller (Table 3 and Figure 5). The diurnal variation pattern also causes a lower DTR in urban than in rural areas (Table 3), which is line in with the findings of Yang, Zhang, et al. (2020). Conversely, the daily amplitude (maximum hourly CUHII minus minimum hourly CUHII) and peak of CUHII vary under the different weather types, being relatively smaller under Types 1, 2, and 5 in comparison to the three other types (Table 3).

### 3.3. Interannual and Intraseasonal Variations of CUHII Related to the Different SWPs

Figures 6 and 7a show the daily, interannual and monthly variation characteristics and monthly frequencies of the six SWPs in the winters of 2012–2017. Obvious interannual and intraseasonal variation characteristics of the SWP types can be seen in the PBL. Type 1 exhibits the highest frequency in winter in Beijing, followed by Type 3, with the lowest frequency appearing in association with Type 6 (Figures 6a and 7a, and Table 2). The days and frequency of Type 1 in the Decembers of 2013, 2016, and 2017 are higher than in other months (Figures 6b and 7a). As the dominant type, Type 1 has the higher frequency in most months (Figures 6c and 7a). These variation characteristics of SWPs in the PBL are potentially modulated by cold-front activities in winter (Figure 3; Y. Yang et al., 2018).

Similarly, Figure 7b shows time series of the monthly averaged CUHII in the winters of 2012–2017, revealing obvious intra seasonal and interannual characteristics of variation. For instance, the monthly averaged CUHII ( $>2^{\circ}\text{C}$ ) in the Decembers of 2013, 2016, and 2017, and Januarys of 2012 and 2018, are higher than in other months. In addition, the CUHIIs in December are mostly higher than those in January and February, showing a decreasing trend from December to February. The causes of these intra seasonal and interannual variations of CUHII need to be further explored, but they may be related to the dominance of certain weather types under the

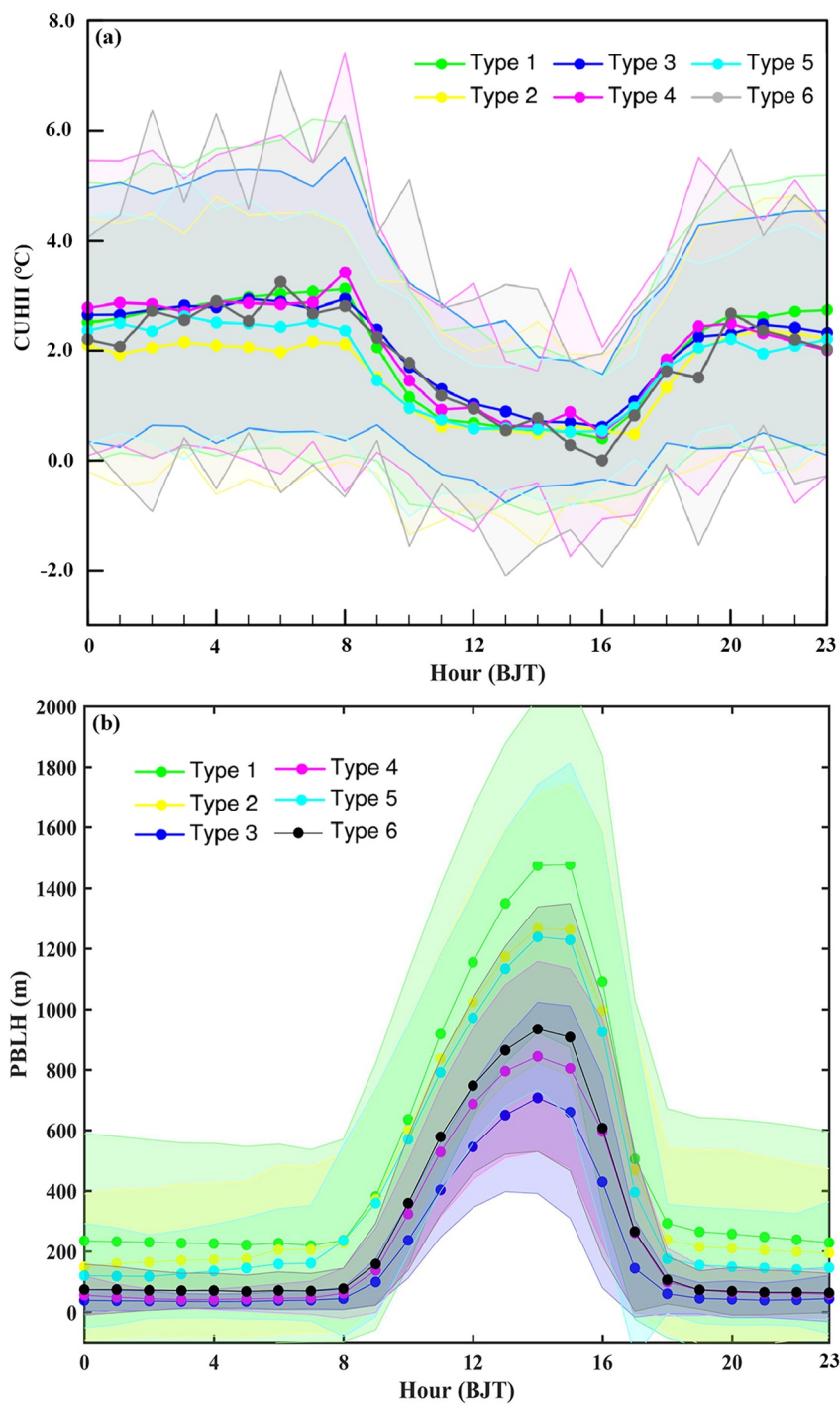


**Figure 5.** (a) Diurnal variation characteristics of the CUHII under the six SWPs in Beijing; (b) Diurnal variation characteristics of the PBLH in urban Beijing.



**Table 3**  
Daily Amplitude of CUHII, and the CUHII<sub>Tmax</sub>, CUHII<sub>Tmin</sub>, DTR<sub>Urban</sub> and DTR<sub>Rural</sub> Under Six Weather Types in Beijing

Type	Daily amplitude (°C)	CUHII <sub>Tmax</sub> (°C)	CUHII <sub>Tmin</sub> (°C)	DTR <sub>Urban</sub> (°C)	DTR <sub>Rural</sub> (°C)
1	2.7	1.2	2.9	9.9	13.0
2	1.9	1.5	2.1	8.7	10.6
3	2.3	1.3	2.9	8.7	11.3
4	2.9	2.2	2.7	10.2	12.6
5	2.1	1.1	2.4	8.5	10.8
6	3.2	1.6	2.5	9.3	11.2

variability of large-scale upper-air circulation in the East Asian region (W. Wang et al., 2021; Y. Yang et al., 2018; Yin et al., 2021).

## 4. Discussion

### 4.1. Roles of Local Wind Speed Modulated by Different SWP<sub>s</sub>

Previous studies have revealed that the CUHII is dependent on the wind speed variation (e.g., discussions in Oke et al., 2017, Yang, Zheng, et al., 2020, and S. Chen et al., 2022). In particular, the CUHII usually decreases as the wind speed increases. Here, Figure 7c shows that there is a significant negative correlation ( $r = -0.38$ ;  $p < 0.05$ ) between the daily averaged CUHII and local wind speed derived from all samples during 2012–2017. Particularly, CUHI were most apparent under weak wind conditions. For the samples in each SWP type, the CUHII also shows a negative correlation with wind

speed. In general, the monthly mean CUHII shows a significant negative correlation ( $r = -0.44$ ;  $p < 0.05$ ) with the monthly mean SWS.

In addition, the rose diagram of maximum daily wind direction and CUHII for different weather types (Figure 8) shows that the CUHII is generally higher when the daily maximum wind speed is lower. For instance, when the wind speeds are concentrated below 2 m/s, the CUHII is usually greater than 2.0°C. In Type 1, Type 2 and Type 5 weather conditions, there are usually strong northwest winds, which is favorable for heat diffusion, and thus the CUHII is smaller (<2°C). Type 3, Type 4, and Type 6 weather conditions are more conducive to heat accumulation and storage, and thus the CUHII tends to be enhanced.

To explore the relationship between the frequency of SWPs and the local wind speed at the interannual scale, Figure 9 shows time series of the monthly frequency of Types 3, 4, and 6 (related to strong CUHII), and Types 1, 2, and 5 (related to weak CUHII) along with the monthly mean wind speeds. There are very high correlation coefficients between the monthly occurrence frequencies of weather types related to strong or weak CUHII and the monthly average SWS (Table 4). Therefore, we can deduce that the interannual variations of CUHII are partly caused by the SWPs via their modulation of the local wind speed.

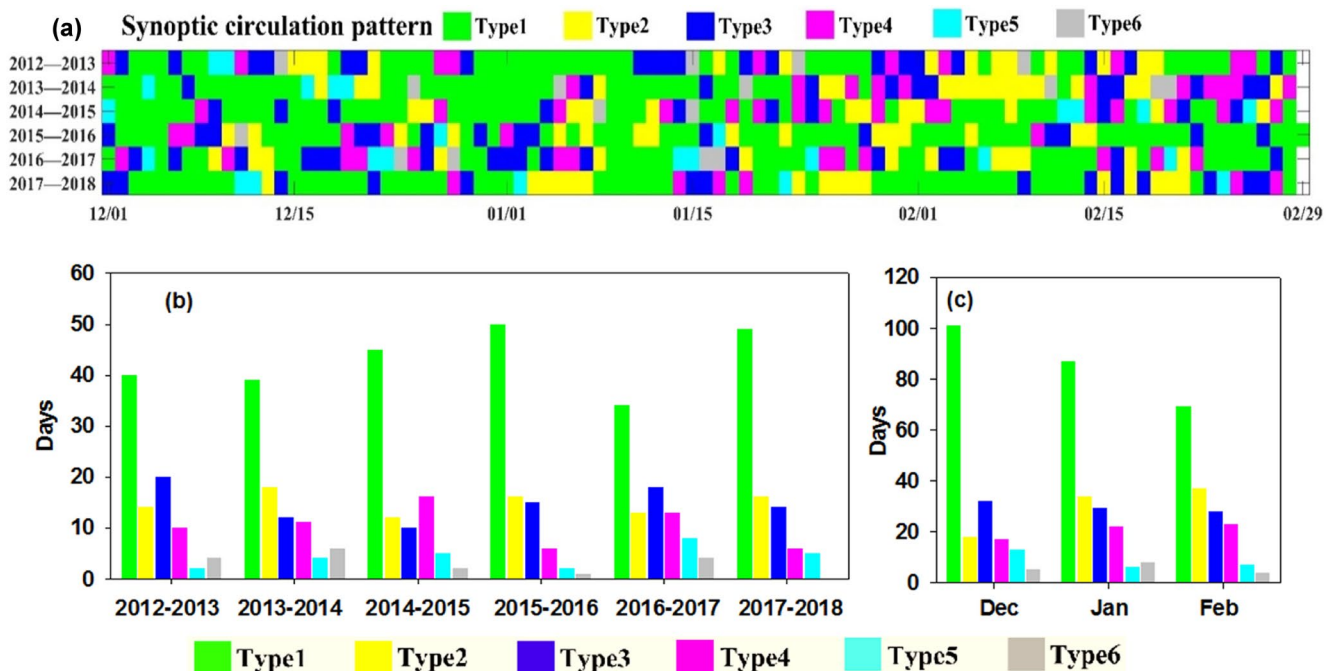


**Figure 6.** (a) Time series of day-to-day variation in SWPs in winter during 2012–2017. (b) Days of each type in every winter during 2012–2017. (c) Mean days of each type in December, January, and February during 2012–2017.

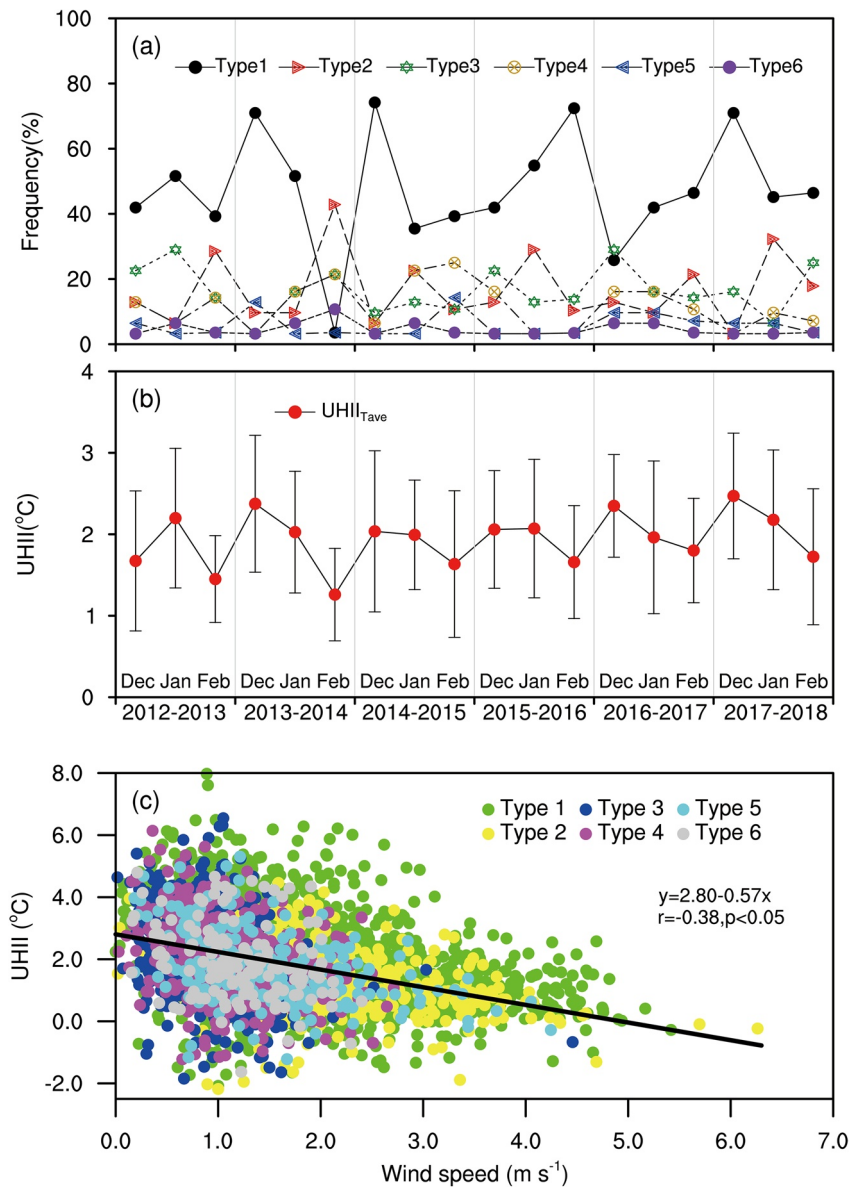


**Figure 7.** (a) Time series of monthly frequency for each SWP and (b) monthly mean CUHII with standard deviation in each winter during 2012–2017. (c) Scatterplot of daily averaged CUHII and wind speed derived from all samples in wintertime during 2012–2017 in Beijing.

The negative relationship between CUHII and local WS in Beijing reported here are consistent with that in other mega cities, that is, CUHII tends to increase with decreasing wind speed, as reported in Tucson (Comrie, 2000), Melbourne (Morries et al., 2001), Singapore (Chow & Roth, 2006), Shanghai (Ao et al., 2019), Berlin (Daniel et al., 2019) and Hong Kong (Wang et al., 2021). In the present work, however, we built a vehicle between various local wind patterns and different SWP in the PBL, which could be useful to understand relationships between synoptic and climatic scales for identifying long-term trends and interannual variability in CUHII in cities.

#### 4.2. Potential Associations With Other Local Meteorological Factors Under Different SWP<sub>s</sub>

Through weather classification, it is found that there are obvious differences in the circulation background under different types, so whether the other local weather conditions under different SWPs will affect CUHII is worth

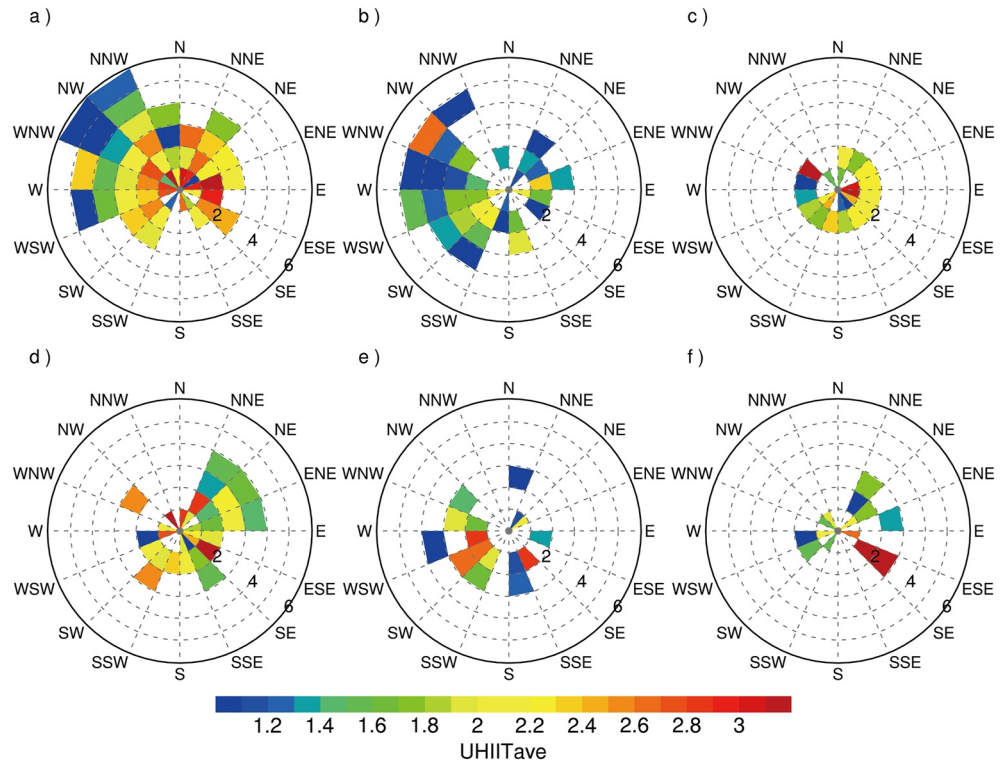


**Figure 8.** Rose diagram of CUHI and wind direction at the maximum daily wind speed (m/s) under various weather types in Beijing [(a–f) indicate Types 1–6, respectively].

noting. In addition to wind vectors, Figures 10–12 show spatial distributions of TCC, precipitation frequency, and PBLH under different SWPs.

Figure 10 shows that there are less TCC under Types 1, 2, and 5. In particular, Type 1 is affected by the strong westerly jet and cloud clusters are unlikely to gather over Beijing, and thus the TCC is abnormally low. Under Types 3, 4, and 6, there are more frequent cloud coverage and higher TCC. Correspondingly, the precipitation frequency distribution (Figure 11) is highly matched with the TCC distribution. Precipitation occurs more frequently in case of the SWPs with large cloud cover. For example, the TCC and precipitation both decreases from the northern to the southern in Type 2. It can also be distinguished according to the magnitude of the precipitation occurrence rate. There are fewer precipitation events at Types 1, 2, and 5, resulting in lower RH (Figure 4), while there are more precipitation events at Types 3, 4, and 6, leading to higher RH (Figure 4). The present SWPs

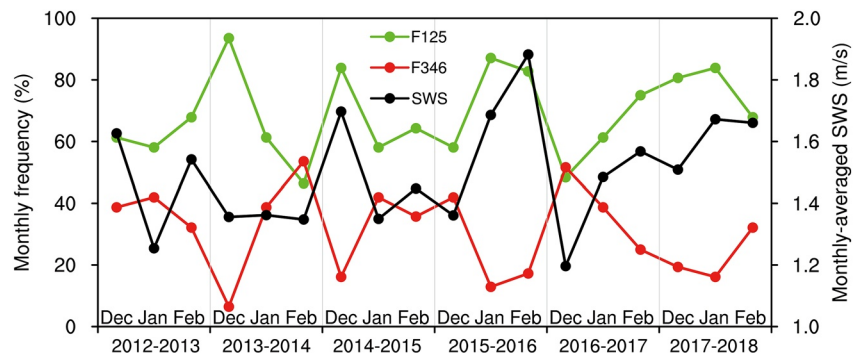


**Figure 9.** Time series of the monthly frequency of Types 3, 4, and 6 (F346; related to strong canopy-level UHII) and Types 1, 2, and 5 (F125; related to weak canopy-level UHII) along with the monthly averaged surface wind speed (SWS) in Beijing.



**Table 4**

Correlation Coefficients of the Monthly Occurrence Frequency of Types 3, 4 and 6 (Related to Strong CUHII), and Types 1, 2, and 5 (Related to Weak CUHII) ( $F_{346}$  and  $F_{125}$ , Respectively), With the Monthly Average CUHII, RH, SWS, and PBLH

	SWS	PBLH	RH
F346	−0.63 <sup>a</sup>	−0.64 <sup>a</sup>	0.78 <sup>a</sup>
F125	0.63 <sup>a</sup>	0.64 <sup>a</sup>	−0.78 <sup>a</sup>

<sup>a</sup>0.01 Confidence.

and their influence on local meteorological factors are consistent with the findings of previous studies (Miao et al., 2019, 2020).

In addition, previous studies have revealed that certain SWPs can suppress the development of the PBL and induce calm, cloudless and heavily polluted conditions (Miao et al., 2019; Y. Yang et al., 2018), which is conducive to CUHII intensification (Cao et al., 2016; Craig & Bornstein, 2002; Stewart & Oke, 2012; Yang, Zheng, et al., 2020). Combining Table 2 and Figure 12, there are high-pressure systems located to the northwest of Beijing under Types 1, 2, and 5, and the associated strong northwesterly dry and cold airflow with high mean wind speed serves to strengthen the boundary layer mixing process. The PBLHs develop higher (Table 2), and the spatial distribution is also relatively similar (Figures 12a, 12b and 12c).

The PBLHs in the north are relatively higher than those in the south. Type 3 is mainly affected by the weaker westerly wind, and the PBLH is the lowest, with most of the area being less than 270 m. However, in Types 4 and 6, the weak high-pressure systems exist to the south of Beijing, resulting in weak prevailing southerly winds with the distribution of PBLH increasing from west to east. Therefore, the PBLH is relatively low due to the weak boundary layer mixing process under the influence of weak high pressure or low pressure (Types 3, 4, and 6). The negative correlation between the monthly mean local PBLH and CUHII is also significant ( $r = -0.44$ ;  $p < 0.05$ ), implying that the lower the PBLH is, the stronger the CUHII is. In addition, Figure 5b shows that diurnal variation of PBLH in urban Beijing also exhibits an opposite trend with that of CUHII in Figure 5a during winter. To explore the relationship between PBLH and SWPs on the interannual scale, we calculated the correlation coefficients between the monthly occurrence frequencies of weather types related to strong or weak CUHII and the monthly average PBLH and RH (Table 4). The interannual variation of the local PBLH is closely related to that of the weather types linked with various CUHII [ $r = -0.64$  (0.64);  $p < 0.01$  (0.01)] (Table 4). In fact, controlled by certain SWP (e.g., Types 3, 4, and 6), low PBLH with strong atmospheric stability are usually associated with weak wind conditions (Figures 4 and 12), which is similar with previous studies (Barlow et al., 2015; W. Wang et al., 2021). Note that PBLH significantly varied with

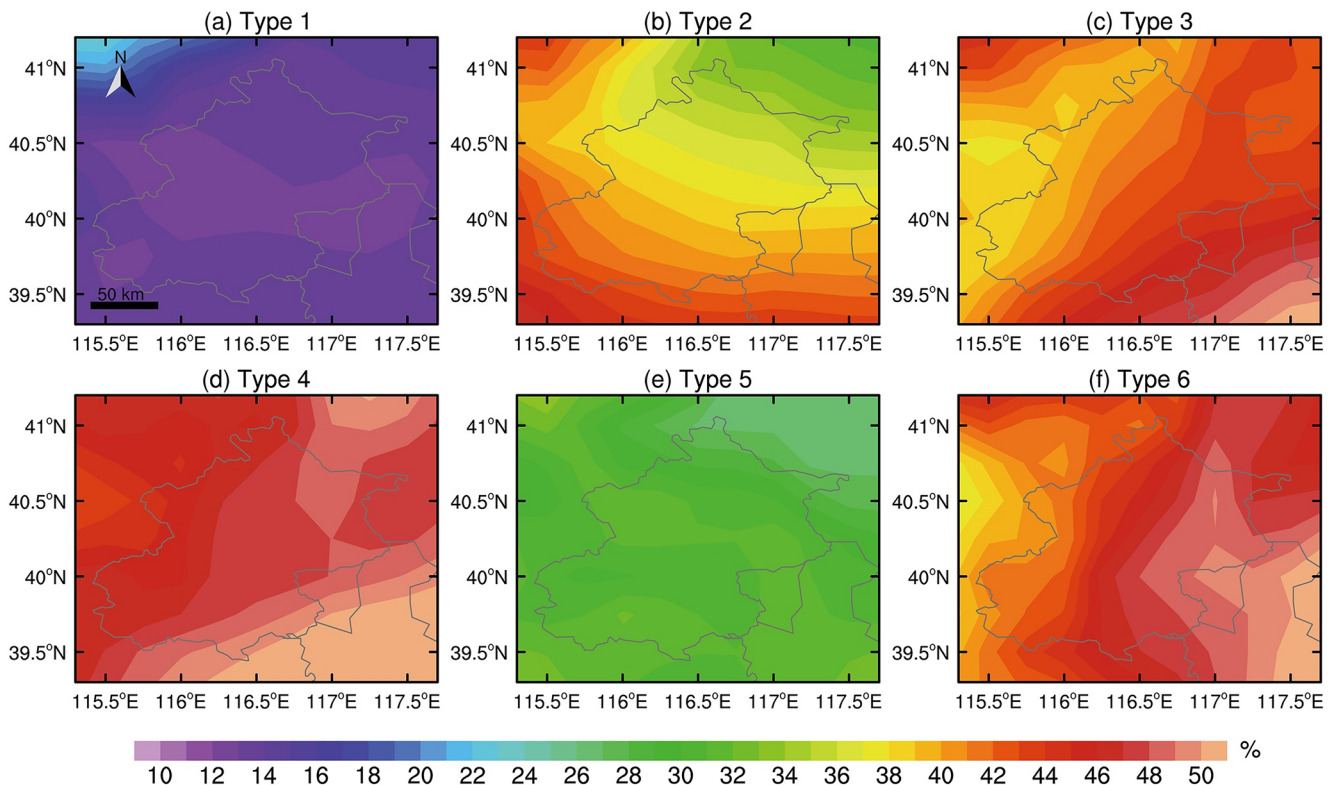


**Figure 10.** Average distribution of the total cloud cover (TCC) in winter under the six SWPs in Beijing [(a–f) indicate Types 1–6, respectively].

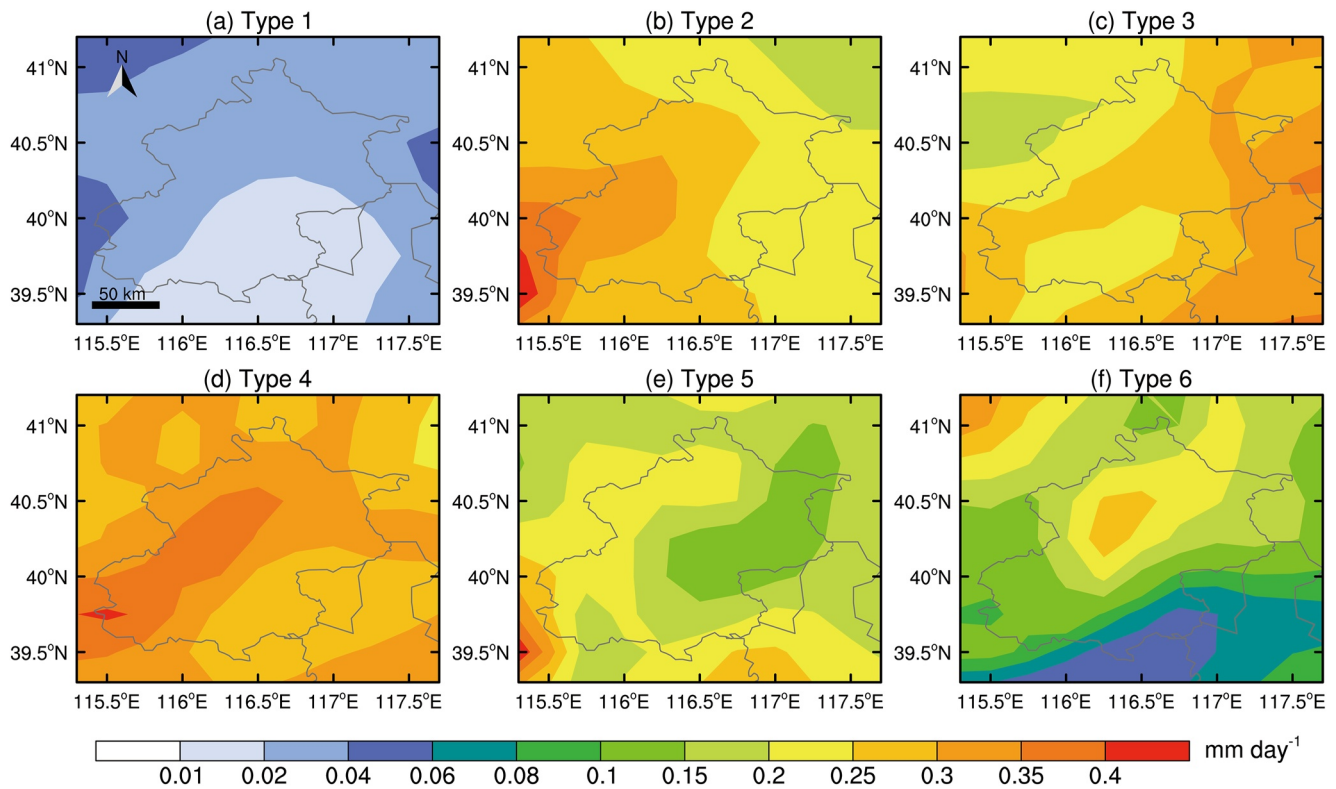


**Figure 11.** Average distribution of the precipitation frequency in winter under the six SWPs in Beijing [(a–f) indicate Types 1–6, respectively].

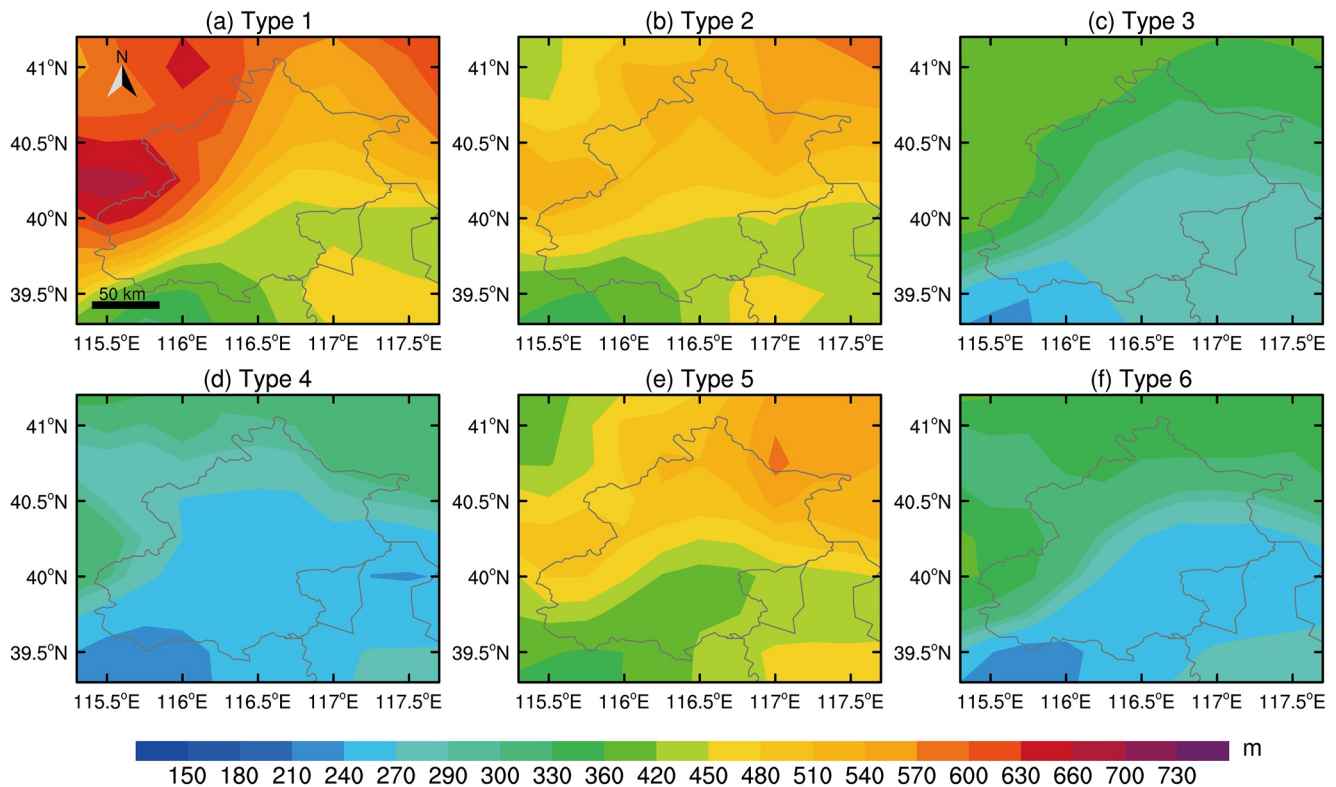


**Figure 12.** Average distribution of the planetary boundary layer height (PBLH) in winter under the six SWPs in Beijing [(a–f) indicate Types 1–6, respectively].

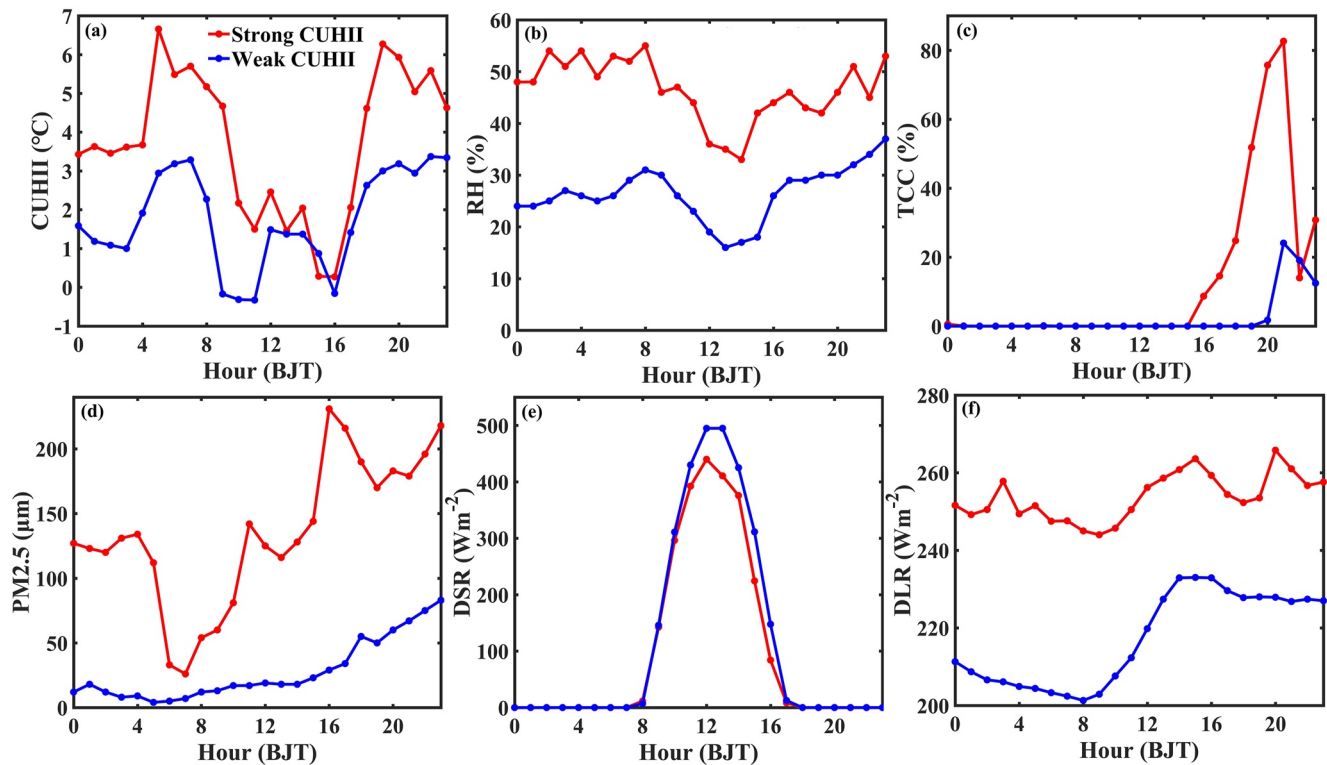


**Figure 13.** Diurnal variations of (a) CUHII, (b) relative humidity (RH), (c) total cloud cover (TCC), (d)  $\text{PM}_{2.5}$  concentration, (e) download shortwave radiation (DSR), (f) download longwave radiation (DLR) during two cases on 07 December 2016 and 14 December 2016, respectively.

season in Beijing (Miao et al., 2015, 2017, 2019), and the relationship between CUHII and PBLH may vary for different seasons, which should be further investigated in future. In addition, there is a significant positive correlation between occurrence frequency of the SWP linked with strong CUHII and RH (Table 4).

In general, under Types 1, 2, and 5, PBLHs develop relatively high, and the strong westerly winds are conducive to the horizontal and vertical diffusion of urban heat (Table 2), alleviating the CUHI effect. In contrast, in the case of Types 3, 4 and 6, weak southerly winds and lower PBLH prevail, which can transport moisture to Beijing, aggravating the accumulation of water vapor, and the resulting higher RH and rain frequency (Table 2 and Figure 11).

Here we have respectively selected two cases of typical strong and weak CUHII to examine the role of downward radiation in the variation of CUHII. In order to eliminate the influence of local wind speed on CUHII, the two cases should be selected for weak wind condition with daily averaged wind speed  $<2$  m/s, referring to the previous study (Yang, Zheng, et al., 2020). Figure 13 shows diurnal variations of CUHII, RH, TCC,  $\text{PM}_{2.5}$  concentration and downward components of radiation under strong CUHII scenario on 07 December 2016 and weak CUHII scenario on 14 December 2016. Relative to weak CUHII case, there were larger quantities of water vapor (higher RH) which can be conducive to the generation of secondary aerosols, and the higher  $\text{PM}_{2.5}$  concentration and TCC at nighttime, in the case of strong CUHII (Figure 13). These conditions are favorable to absorb longwave radiation emitted by the surface to heat the atmosphere and to emit more downward longwave radiation (Li, Zhou, et al., 2020; Yang, Zheng, et al., 2020; Zheng et al., 2018), which reduces the loss of surface longwave radiation and resultantly enhances the nighttime CUHII. At daytime, however, with the increase of  $\text{PM}_{2.5}$  concentration, which can reduce downward shortwave radiation through absorbing and scattering effect, there is a weak daytime CUHII, especially during 1200–1600 BJT on 7 December (Figure 13). The present results are also consistent with the previous analyses (Li, Zhou, et al., 2020; Yang, Wu, et al., 2013; Yang, Zheng, et al., 2020; Zheng et al., 2018). The daytime–nighttime difference in CUHII related to air pollution under different SWPs can be also estimated according to the diurnal variation characteristics of the CUHII shown in Figure 5.



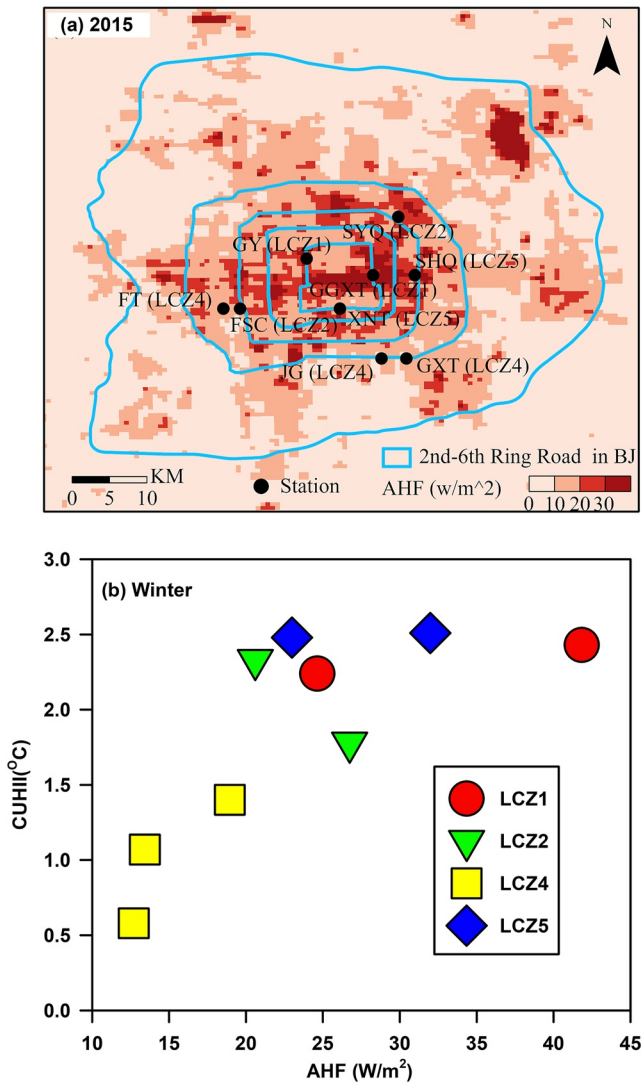


**Figure 14.** (a) The distribution map of anthropogenic heat flux in 2015 and (b) scatterplot of relationships between CUHII and AHF over different LCZs in winter during 2012–2017.

Generally, it can be deduced that the various SWPs modulate the local SWS with varying PBLH, cloud cover, and RH to affect the interannual and diurnal variation of the CUHII.

#### 4.3. Modulations of AHF in Different Local Climate Zones

Previous studies indicated that urbanization factors (e.g., urban land-use changes, anthropogenic heat emissions, urban morphology and size) influence the CUHII of complex and diverse cities (Li, Schubert, et al., 2020; Manoli et al., 2019; Roth, 2007; K. Wang et al., 2017; N. Zhang et al., 2015; Zong, Liu, et al., 2021). Particularly, the Anthropogenic Heat Flux (AHF) is closely related to the change of built-up areas and population density around the stations, which can be considered to reflect the effects of both anthropogenic emission and land use change which are related to latent heat flux and sensible heat flux (L. Wang et al., 2020; Yang, Zhang, et al., 2020; Y. Zhang et al., 2021). For spatial patterns of CUHII, therefore, we further discussed the link of mean CUHII over different LCZs with various AHFs. Figure 14 shows the relationships between CUHII and AHF over different LCZs. Generally, strong CUHII are corresponding to the areas of high AHF ( $>10 W/m^2$ ) and high fraction of built-up area (Figures 1, 4 and 14). CUHII significantly decrease with decreasing AHF and increasing distance to the urban center, with a stepdown trend of  $LCZ1 > LCZ5 > LCZ2 > LCZ4$ . Particularly, stronger CUHII occurs in both dense high-rise building and high AHF ( $>40 W/m^2$ ) areas (i.e., LCZ1, GGXT station in Figure 14a).

Differently, although LCZ5 stands for an open mid-rise building area, for example, SHQ station, the strongest CUHII still appears over there when there is higher AHF near the urban center. To explain this, the specific order of the AHFs of the six stations of LCZ1, LCZ2, and LCZ5 is given as follows: GGXT(LCZ1)  $>$  SHQ(LCZ5)  $>$  SYQ(LCZ2)  $>$  GY(LCZ1)  $>$  XNT(LCZ5)  $>$  FSC(LCZ2). It is notable that the AHF of the two stations of LCZ5 and the SYQ station of LCZ2 is quite high. Figure 1b shows that SHQ station is close to the East Fourth Ring Road and a complex overpass, XNT station is close to the South Second Ring Road, and SYQ station is close to the North Fourth Ring Road and another complex overpass. Therefore, vast heat emissions from the heavy traffic may be the reason for the high AHF at these three stations. In addition, there are more vegetation in the east of GY station in LCZ1, which may be conducive to the reduction of the AHF and the increase of latent heat flux around the station.

#### 4.4. Implications and Limitations

Air temperature change has a direct and strong correlation with energy consumption. Previous studies examined the relationships between UHIs and the energy consumption of cities in northern China, indicating that for every increase of  $1^{\circ}C$  in UHII, the average annual heating loads of the city will be decreased by  $4.01 kWh/m^2$  in winter, while the annual average cooling loads will be increased by  $1.05 kWh/m^2$  in summer (Meng, Guo, et al., 2020; Meng, Ren, et al., 2020). In our present work, it can be concluded that local climate zones organized by anthropogenic factors largely modulate the dominant spatial pattern of CUHII, while different SWPs influence the temporal variation in strength of CUHII during winter in Beijing. Recent study pointed out that urban climate research should be aimed to reduce the impacts of urban heat rather than to mitigate the UHI magnitude (Martilli et al., 2020). Our findings can provide a reference base for policy and technical guidelines for urban planning in northern high-density cities. For instance, in winter, we can make a dynamic policy decision for energy-saving and habitat comfort, that is, the energy supply for heating loads can be reduced in real time under SWPs conditions related to strong CUHII over urban areas, especially over dense high-rise building and high AHF areas of the urban center (e.g., LCZ1, LCZ2, LCZ3), and vice versa. While in summer, the heat mitigation strategies

should be focused on suppression of anthropogenic heat emissions and heat storages over urban areas (Martilli et al., 2020; Yang & Bou-Zeid, 2019; J. Yang et al., 2016). At least, electricity consumption for cooling in public and official buildings can be reduced in real time under SWPs conditions related to weak CUHI over urban areas, and vice versa. These measures will be also beneficial to improve urban air quality, due to less pollutant emissions from both reduced heating and cooling.

This study of CUHI based on SWP and LCZ classifications could be extended to other similar large cities in the world. However, the physical mechanisms underpinning the interactions between the CUHI and local meteorological factors as modulated by SWPs, as well as the related coping strategies, may need to be carefully addressed by considering different conditions of climate, geography and urban fabric and structure. In addition, it should be interesting to further examine the LCZs that exhibit the strongest CUHI effect by season and weather type in our next work.

## 5. Conclusions

The present work systematically explores the associations between CUHI and SWPs in the PBL and their potential drivers by using multi-source meteorological and environmental data, as well as reanalysis data, together with the T-PCA method. The main conclusions can be summarized as follows:

Based on the T-PCA results, six dominant types of SWP during the wintertime of the period 2012–2017 can be identified. Under Types 1, 2, and 5, high-pressure systems are located to the northwest of Beijing, and the associated strong northwest dry and cold airflows with high wind speeds serve to strengthen the boundary layer mixing process. Strong dry and cold airflows result in less precipitation and more clearing weather. In contrast, in the case of Types 3, 4, and 6, weak high-pressure systems exist to the south of Beijing, resulting in prevailing weak southerly winds with low PBLH. These weather patterns are usually accompanied by more frequent precipitation and more cloud cover. Our findings suggest that the impacts of SWPs on the wintertime CUHI take place mainly via their modulation of local winds, the PBLH, cloud and RH, at diurnal and interannual scales, with winds being the dominant factor. For instance, a strengthened CUHI is accompanied by three SWPs (Types 3, 4, 6) with a lower SWS and PBLH, and higher RH; whereas, a decreased CUHI is accompanied by three SWPs (Types 1, 2, 5) with a higher SWS and PBLH, and lower RH. The daily amplitudes and peaks of CUHI vary under the different weather types, being relatively smaller under Types 1, 2, and 5 with respect to the other three types. In addition, spatial patterns of CUHI in Beijing are highly correlated with areas of high AHF ( $>10 \text{ W/m}^2$ ) and high fraction of built-up area. Generally, local climate zones organized by anthropogenic factors modulate the dominant spatial pattern of CUHI, while different weather types influence the magnitude of CUHI at diurnal and interannual scales.

Broadly, our findings have implications for CUHI forecasts, as well as impact assessments and policymaking in the context of CUHI-related energy conservation in winter and summer, and CUHI-induced high-temperature disasters in summer over high-density urban areas on the synoptic scale. Our research demonstrates that both natural variability (e.g., SWPs) and human activities (e.g., LCZ related to urbanization) play important roles in formation and development of CUHI against the complex background of land–atmosphere–anthroposphere coupling.

## Data Availability Statement

The data that support the findings of this study are openly available as followings. The ground-based meteorological data are deposited at linkage: <https://doi.org/10.5281/zenodo.5893959> (Yang, 2022). NCEP provided the (global FNL) reanalysis data (<https://doi.org/10.5065/D6M043C6>). ECMWF provided the ERA5 reanalysis data (<https://doi.org/10.24381/cds.bd0915c6>).

## Acknowledgments

This study was supported by the National Natural Science Foundation of China (42175098), the National Key R&D Program of China (Fund No: 2018YFA0605603), and the Beijing Natural Science Foundation (8202022).

## References

- Ao, X. Y., Wang, L., Zhi, X., Gu, W., Yang, H. Q., & Li, D. (2019). Observed synergies between urban heat islands and heat waves and their controlling factors in Shanghai, China. *Journal of Applied Meteorology and Climatology*, 58, 1955–1972. <https://doi.org/10.1175/JAMC-D-19-0073.1>
- Barlow, J. F., Halios, C. H., Lane, S. E., & Wood, C. R. (2015). Observations of urban boundary layer structure during a strong urban heat island event. *Environmental Fluid Mechanics*, 15, 373–398. <https://doi.org/10.1007/s10652-014-9335-6>

- Cao, C., Lee, X., Liu, S. D., Schultz, N., Xiao, W., Zhang, M., & Zhao, L. (2016). Urban heat islands in China enhanced by haze pollution. *Nature Communications*, 7, 12509. <https://doi.org/10.1038/ncomms12509>
- Chen, L., Zhang, M., Zhu, J., Wang, Y., & Skorokhod, A. (2018). Modeling impacts of urbanization and urban heat island mitigation on boundary layer meteorology and air quality in Beijing under different weather conditions. *Journal of Geophysical Research: Atmospheres*, 123(8), 4323–4344. <https://doi.org/10.1002/2017JD027501>
- Chen, S., Yang, Y., Deng, F., Zhang, Y., Liu, D., Liu, C., & Gao, Z. (2022). A high-resolution monitoring approach of canopy urban heat island using random forest model and multi-platform observations. *Atmospheric Measurement Techniques*, 15. <https://doi.org/10.5194/amt-2021-301>
- Chen, S. S., Hu, D., Wong, M. S., Ren, H., Cao, S., Yu, C., & Ho, H. C. (2019). Characterizing spatiotemporal dynamics of anthropogenic heat fluxes: A 20-year case study in Beijing-Tianjin-Hebei region in China. *Environmental Pollution*, 249, 923–931. <https://doi.org/10.1016/j.envpol.2019.03.113>
- Chow, W., & Roth, M. (2006). Temporal dynamics of the urban heat island of Singapore. *International Journal of Climatology*, 26, 2243–2260. <https://doi.org/10.1002/joc.1364>
- Comrie, A. C. (2000). Mapping a wind-modified urban heat island in Tucson, Arizona. *Bulletin of the American Meteorological Society*, 81, 2417–2431. [https://doi.org/10.1175/1520-0477\(2000\)081<2417:mawmuh>2.3.co;2](https://doi.org/10.1175/1520-0477(2000)081<2417:mawmuh>2.3.co;2)
- Craig, K., & Bornstein, R. (2002). MM5 simulation of urban induced convective precipitation over Atlanta. In *Paper presented at fourth conference on the urban environment* (pp. 20–24). Norfolk, Va: American Meteorological Society.
- Crutzen, P. J. (2004). New direction: The growing urban heat and pollution “island” effect—impact on the chemistry and climate. *Atmospheric Environment*, 38, 3539–3540. <https://doi.org/10.1016/j.atmosenv.2004.03.032>
- Cui, Y., Yan, D., Hong, T., & Ma, J. (2017). Temporal and spatial characteristics of the urban heat island in Beijing and the impact on building design and energy performance. *Energy*, 130, 286–297. <https://doi.org/10.1016/j.energy.2017.04.053>
- Daniel, F., Holtmann, A., Meier, F., Langer, I., & Scherer, D. (2019). Contrasting changes of urban heat island intensity during hot weather episodes. *Environmental Research Letters*, 12, 124013. <https://doi.org/10.1088/1748-9326/ab506b>
- Hoffmann, P., & Heinke Schlünzen, K. (2013). Weather pattern classification to represent the urban heat island in present and future climate. *Journal of Applied Meteorology and Climatology*, 52(12), 2699–2714. <https://doi.org/10.1175/JAMC-D-12-065.1>
- Hu, K. J., Guo, Y. M., Hochrainer-Stigler, S., Liu, W., See, L., Yang, X. C., et al. (2019). Evidence for urban–rural disparity in temperature–mortality relationships in Zhejiang Province, China. *Environmental Health Perspectives*, 127(3), 037001. <https://doi.org/10.1289/EHP3556>
- Jauregui, E., Godínez, L., & Cruz, F. (1992). Aspects of heat-island development in Guadalajara, Mexico. *Atmospheric Environment*, 26(3), 391–396. [https://doi.org/10.1016/0957-1272\(92\)90014-j](https://doi.org/10.1016/0957-1272(92)90014-j)
- Kolokotroni, M., Ren, X., Davies, M., & Mavrogiani, A. (2012). London’s urban heat island: Impact on current and future energy consumption in office buildings. *Energy and Buildings*, 47, 302–311. <https://doi.org/10.1016/j.enbuild.2011.12.019>
- Li, D., & Bouzeid, E. (2013). Synergistic interaction between urban heat islands and heat waves: The impact in cities is larger than the sum of its parts. *Journal of Applied Meteorology and Climatology*, 52(9), 2051–2064. <https://doi.org/10.1175/jamc-d-13-02.1>
- Li, J., Zhou, M., Lenschow, D. H., Cheng, Z., & Dou, Y. (2020). Observed relationships between the urban heat island, urban pollution island, and downward longwave radiation in the Beijing area. *Earth and Space Science*, 7(6). <https://doi.org/10.1029/2020EA001100>
- Li, Y., Schubert, S., Kropp, J. P., & Rybski, D. (2020). On the influence of density and morphology on the urban heat island intensity. *Nature Communications*, 11, 2647. <https://doi.org/10.1038/s41467-020-16461-9>
- Liu, S. H., Liu, Z. X., Li, J., Wang, Y. C., Ma, Y. J., Sheng, L., et al. (2009). Numerical simulation for the coupling effect of local atmospheric circulations over the area of Beijing, Tianjin and Hebei Province. *Science in China—Series E: Technological Sciences*, 52(3), 382–392. <https://doi.org/10.1007/s11430-009-0030-2>
- Liu, W., Ji, C., Zhong, J., Jiang, X., & Zheng, Z. (2007). Temporal characteristics of the Beijing urban heat island. *Theoretical and Applied Climatology*, 87(4), 213–221. <https://doi.org/10.1007/s00704-005-0192-6>
- Luo, M., & Lau, N. C. (2017). Heat waves in Southern China: Synoptic behavior, long-term change and urbanization effects. *Journal of Climate*, 30(2), 703–720. <https://doi.org/10.1175/JCLI-D-16-0269.1>
- Luo, M., & Lau, N. C. (2018). Increasing heat stress in urban areas of eastern China: Acceleration by urbanization. *Geophysical Research Letters*, 45(23), 13060–13069. <https://doi.org/10.1029/2018GL080306>
- Manoli, G., Faticchi, S., Schläpfer, M., Yu, K., Crowther, T. W., Meili, N., et al. (2019). Magnitude of urban heat islands largely explained by climate and population. *Nature*, 573, 55–60. <https://doi.org/10.1038/s41586-019-1512-9>
- Martilli, A., Krayenhoff, E. S., & Nazarian, N. (2020). Is the Urban Heat Island intensity relevant for heat mitigation studies? *Urban Climate*, 31, 100541. <https://doi.org/10.1016/j.uclim.2019.100541>
- Max, A., Targino, A. C., Krecl, P., Oukawa, G. Y., & Braga, R. F. (2020). Analysis of the urban heat island under different synoptic patterns using local climate zones. *Building and Environment*, 185, 107268. <https://doi.org/10.1016/j.buildenv.2020.107268>
- Meng, F., Guo, J., Ren, G., Zhang, L., & Zhang, R. (2020). *Impact of Urban Heat Island on the Variation of Heating Loads in Residential and Office Buildings in Tianjin* (Vol. 226). Energy & Buildings. <https://doi.org/10.1016/j.enbuild.2020.110357>
- Meng, F., Ren, G., Guo, J., Zhang, L., & Zhang, R. (2020). Impact of urban heat island effect on the heating and cooling loads of residential buildings in Tianjin City, China. *Progress in Geography*, 39(8), 1296–1307. <https://doi.org/10.18306/dlkxjz.2020.08.005>
- Miao, Y., Che, H., Zhang, X., & Liu, S. (2020). Integrated impacts of synoptic forcing and aerosol radiative effect on boundary layer and pollution in the Beijing–Tianjin–Hebei region, China. *Atmospheric Chemistry and Physics*, 20(10), 5899–5909. <https://doi.org/10.5194/acp-20-5899-2020>
- Miao, Y., Guo, J., Liu, S., Liu, H., Li, Z., Zhang, W., & Zhai, P. (2017). Classification of summertime synoptic patterns in Beijing and their associations with boundary layer structure affecting aerosol pollution. *Atmospheric Chemistry and Physics*, 17(4), 3097–3110. <https://doi.org/10.5194/acp-17-3097-2017>
- Miao, Y., Hu, X.-M., Liu, S., Qian, T., Xue, M., Zheng, Y., & Wang, S. (2015). Seasonal variation of local atmospheric circulations and boundary layer structure in the Beijing-Tianjin-Hebei region and implications for air quality. *Journal of Advances in Modeling Earth Systems*, 7, 1602–1626. <https://doi.org/10.1002/2015MS000522>
- Miao, Y., Liu, S., & Huang, S. (2019). Synoptic pattern and planetary boundary layer structure associated with aerosol pollution during winter in Beijing, China. *The Science of the Total Environment*, 682, 464–474. <https://doi.org/10.1016/j.scitotenv.2019.05.199>
- Morris, C. J. G., Simmonds, I., & Plummer, N. (2001). Quantification of the influences of wind and cloud on the nocturnal urban heat island of a large city. *Journal of Applied Meteorology*, 40(2), 169–182. [https://doi.org/10.1175/1520-0450\(2001\)040<0169:qotow>2.0.co;2](https://doi.org/10.1175/1520-0450(2001)040<0169:qotow>2.0.co;2)
- Muñoz-Sabater, J., Dutra, E., Agustí-Panareda, A., Albergel, C., Arduini, G., Balsamo, G., et al. (2021). ERA5-Land: A state-of-the-art global reanalysis dataset for land applications. *Earth System Science Data*, 13, 4349–4383. <https://doi.org/10.5194/essd-13-4349-2021>
- National Centers for Environmental Prediction/National Weather Service/NOAA/U.S. Department of Commerce. (2000). *NCEP FNL Operational Model Global Tropospheric Analyses*. UCAR/NCAR - Research Data Archive. <https://doi.org/10.5065/D6M043C6>



- Ning, G., Wang, S., Yim, S. H. L., Li, J., Hu, Y., Shang, Z., et al. (2018). Impact of low-pressure systems on winter heavy air pollution in the northwest Sichuan Basin, China. *Atmospheric Chemistry and Physics*, 18(18), 13601–13615. <https://doi.org/10.5194/acp-18-13601-2018>
- Ning, G., Yim, S. H. L., Wang, S., Duan, B., Nie, C., Yang, X., et al. (2019). Synergistic effects of synoptic weather patterns and topography on air quality: A case of the sichuan basin of China. *Climate Dynamics*, 53(11), 6729–6744. <https://doi.org/10.1007/s00382-019-04954-3>
- Oke, T. R., Johnson, G. T., Steyn, D. G., & Watson, I. D. (1991). Simulation of surface urban heat islands under 'ideal' conditions at night. Part 2: Diagnosis of causation. *Boundary-Layer Meteorology*, 56, 339–358. <https://doi.org/10.1007/bf00119211>
- Oke, T. R., & Maxwell, G. B. (1975). Urban heat island dynamics in Montreal and Vancouver. *Atmospheric Environment*, 9(2), 191–200. [https://doi.org/10.1016/0004-6981\(75\)90067-0](https://doi.org/10.1016/0004-6981(75)90067-0)
- Oke, T. R., Mills, G., Christen, A., & Voogt, J. A. (2017). *Urban climates* (p. 157). Cambridge University Press.
- Philipp, A., Beck, C., Esteban, P., Krennert, T., Lochbihler, K., Spyros, P., et al. (2014). *Cost733 user guide*.
- Ren, G. Y. (2015). Urbanization as a major driver of urban climate change. *Advances in Climate Change Research*, 6(1), 1–6. <https://doi.org/10.1016/j.accre.2015.08.003>
- Ren, G. Y., Chu, Z. Y., Chen, Z. H., & Ren, Y. Y. (2007). Implications of temporal change in urban heat island intensity observed at Beijing and Wuhan stations. *Geophysical Research Letters*, 34, L05711. <https://doi.org/10.1029/2006gl027927>
- Rizwan, A. M., Dennis, L. Y. C., & Liu, C. (2008). A review on the generation, determination and mitigation of urban heat island. *Journal of Ecology and Environmental Sciences*, 20, 120–128. [https://doi.org/10.1016/s1001-0742\(08\)60019-4](https://doi.org/10.1016/s1001-0742(08)60019-4)
- Roth, M. (2007). Review of urban climate research in (sub) tropical regions. *International Journal of Climatology*, 27(14), 1859–1873. <https://doi.org/10.1002/joc.1591>
- Smith, C. A., Compo, G. P., & Hooper, D. K. (2014). Web-based Reanalysis Intercomparison Tools (WRIT) for analysis and comparison of reanalyses and other datasets. *Bulletin of the American Meteorological Society*, 95(11), 1671–1678. <https://doi.org/10.1175/bams-d-13-00192.1>
- Stewart, I. D., & Oke, T. R. (2012). Local climate zones for urban temperature studies. *Bulletin America Meteorology Social*, 93(12), 1879–1900. <https://doi.org/10.1175/BAMS-D-11-00019.1>
- Sun, Y., & Augenbroe, G. (2014). Urban heat island effect on energy application studies of office buildings. *Energy and Buildings*, 77, 171–179. <https://doi.org/10.1016/j.enbuild.2014.03.055>
- Velasco, E., & Roth, M. (2012). Review of Singapore's air quality and greenhouse gas emissions: Current situation and opportunities. *Journal of the Air & Waste Management Association*, 62(6), 625–641. <https://doi.org/10.1080/10962247.2012.666513>
- Wang, K., Jiang, S., Wang, J., Zhou, C., Wang, X., & Lee, X. (2017). Comparing the diurnal and seasonal variabilities of atmospheric and surface urban heat islands based on the Beijing urban meteorological network. *Journal of Geophysical Research: Atmospheres*, 122, 2131–2154. <https://doi.org/10.1002/2016jd025304>
- Wang, L., Fan, S. H., Hu, F., Miao, S., Yang, A. Q., Li, Y. B., et al. (2020). Vertical Gradient variations in radiation budget and heat fluxes in the urban boundary layer: A comparison study between polluted and clean air episodes in Beijing during winter. *Journal of Geophysical Research: Atmospheres*, 125. <https://doi.org/10.1029/2020jd032478>
- Wang, W., Chen, B., Xu, Y., Zhou, W., & Wang, X. (2021). Urban heat islands in Hong Kong: Bonding with atmospheric stability. *Atmospheric Science Letters*, 22. <https://doi.org/10.1002/asl.1032>
- Xie, Z., Cui, J. L., Chen, D. G., & Hu, B. K. (2006). The annual, seasonal and monthly characteristics of diurnal variation of urban heat island intensity in Beijing. *Environmental Research: Climate*, 11(1), 69–75.
- Xu, W., Li, Q., Wang, X., Yang, S., Cao, L., & Feng, Y. (2013). Homogenization of Chinese daily surface air temperatures and analysis of trends in the extreme temperature indices. *Journal of Geophysical Research: Atmospheres*, 118, 1–9720. <https://doi.org/10.1002/jgrd.50791>
- Yan, Z. W., Li, Z., Li, Q. X., & Jones, P. (2010). Effects of site-change and urbanisation in the Beijing temperature series 1977–2006. *International Journal of Climatology*, 30(8), 1226–1234. <https://doi.org/10.1002/joc.1971>
- Yang, J., & Bou-Zeid, E. (2019). Scale dependence of the benefits and efficiency of green and cool roofs. *Landscape and Urban Planning*, 185, 127–140. <https://doi.org/10.1016/j.landurbplan.2019.02.004>
- Yang, J., Wang, Z. H., Kaloush, K. E., & Dylla, H. (2016). Effect of pavement thermal properties on mitigating urban heat islands: A multi-scale modeling case study in Phoenix. *Building and Environment*, 108, 110–121. <https://doi.org/10.1016/j.buildenv.2016.08.021>
- Yang, P., Ren, G. Y., & Hou, W. (2019). *Impact of Daytime Precipitation Duration on Urban Heat Island Intensity over Beijing City* (Vol. 28). Urban Climate. <https://doi.org/10.1016/j.uclim.2019.100463>
- Yang, P., Ren, G. Y., & Liu, W. D. (2013). Spatial and temporal characteristics of Beijing urban heat island intensity. *Journal of Applied Meteorology*, 52(8), 1803–1816. <https://doi.org/10.1175/jamc-d-12-0125.1>
- Yang, X. C., Leung, L. R., Zhao, N. Z., Zhao, C., Qian, Y., Hu, K. J., et al. (2017). Contribution of urbanization to the increase of extreme heat events in an urban agglomeration in East China. *Geophysical Research Letters*, 44, 6940–6950. <https://doi.org/10.1002/2017gl074084>
- Yang, Y. (2022). *Ground-based data from the article "Modulation of wintertime Canopy Urban Heat Island (CUHI) intensity in Beijing by synoptic weather pattern in planetary boundary layer"*. Zenodo. <https://doi.org/10.5281/ZENODO.5893959>
- Yang, Y., Zhang, M., Li, Q. X., Chen, B., Gao, Z. Q., Ning, G. C., et al. (2020). Modulations of surface thermal environment and agricultural activity on intraseasonal variations of summer diurnal temperature range in the Yangtze River Delta of China. *The Science of the Total Environment*, 736, 139445. <https://doi.org/10.1016/j.scitotenv.2020.139445>
- Yang, Y., Zheng, X., Gao, Z., Wang, H., Wang, T., Li, Y., et al. (2018). Long-term trends of persistent synoptic circulation events in planetary boundary layer and their relationships with haze pollution in winter Half Year over Eastern China. *Journal of Geophysical Research: Atmospheres*, 123, 10–991. <https://doi.org/10.1029/2018jd028982>
- Yang, Y., Zheng, Z., Yim, S. H. L., Roth, M., Ren, G., Gao, Z., et al. (2020). PM2.5 Pollution modulates wintertime urban-heat-island intensity in the Beijing-Tianjin-Hebei megalopolis, China. *Geophysical Research Letters*, 47(1). <https://doi.org/10.1029/2019gl084288>
- Yang, Y. J., Gao, Z. Q., Shi, T., Wang, H., Li, Y. B., Zhang, N., et al. (2019). Assessment of urban surface thermal environment using MODIS with population-weighted method: A case study. *Journal of Spatial Science*, 64, 287–300. <https://doi.org/10.1080/14498596.2017.1422155>
- Yang, Y. J., Wu, B. W., Shi, C. E., Zhang, J. H., Li, Y. B., Tang, W. A., et al. (2013). Impacts of urbanization and station-relocation on surface air temperature series in Anhui Province, China. *Pure and Applied Geophysics*, 170. <https://doi.org/10.1007/s00024-012-0619-9>
- Yin, Z. C., Zhou, B. T., Chen, H. P., & Li, Y. Y. (2021). Synergetic impacts of Precursory climate drivers on interannual-decadal variations in haze pollution in North China: A review. *Science of the Total Environment*, 755, 143017. <https://doi.org/10.1016/j.scitotenv.2020.143017>
- Zhang, L., Ren, G. Y., Liu, J., Zhou, Y. Q., Ren, Y. Y., Zhang, A. Y., & Feng, Y. W. (2011). Urban effect on trends of extreme temperature indices at Beijing Meteorological Station. *Chinese Journal of Geophysics*, 54(5), 1150–1159.
- Zhang, N., Wang, X., Chen, Y., Dai, W., & Wang, X. (2015). Numerical simulations on influence of urban land cover expansion and anthropogenic heat release on urban meteorological environment in Pearl River Delta. *Theoretical and Applied Climatology*, 126, 469–479. <https://doi.org/10.1007/s00704-015-1601-0>

- Zhang, Y., Ning, G., Chen, S., & Yang, Y. (2021). Impact of rapid urban sprawl on the local meteorological observational environment based on remote sensing images and GIS Technology. *Remote Sensing*, 13(13), 2624. <https://doi.org/10.3390/rs13132624>
- Zhao, L., Lee, X., Smith, R. B., & Oleson, K. (2014). Strong contributions of local background climate to urban heat islands. *Nature*, 511, 216–219. <https://doi.org/10.1038/nature13462>
- Zheng, Z. F., Ren, G. Y., Wang, H., Dou, J. X., Gao, Z. Q., Duan, C. F., et al. (2018). Relationship between fine particle pollution and the urban heat island in Beijing, China: Observational evidence. *Boundary Layer Meteorology*, 169(1), 93–113. <https://doi.org/10.1007/s10546-018-0362-6>
- Zheng, Z. F., Zhao, C., Lolli, S., Wang, X. D., Wang, Y. T., Ma, X. Y., et al. (2020). Diurnal variation of summer precipitation modulated by air pollution: Observational evidences in the Beijing metropolitan area. *Environmental Research Letters*, 15. <https://doi.org/10.1088/1748-9326/ab99fc>
- Zong, L., Liu, S., Yang, Y., Ren, G., Yu, M., Zhang, Y., & Li, Y. (2021). Synergistic influence of local climate zones and wind speeds on the urban heat island and heat waves in the megacity of Beijing, China. *Frontiers in Earth Science*, 9. <https://doi.org/10.3389/feart.2021.673786>
- Zong, L., Yang, Y., Gao, M., Wang, H., Wang, P., Zhang, H., et al. (2021). Large-scale synoptic drivers of co-occurring summertime ozone and PM2.5 pollution in eastern China. *Atmospheric Chemistry and Physics*, 21, 9105–9124. <https://doi.org/10.5194/acp-21-9105-2021>